Physico-chemical profiles of the wobble↔Watson–Crick G*·2AP(w)↔G·2AP(WC) and A·2AP(w)↔A*·2AP(WC) tautomerisations: A QM/QTAIM comprehensive survey

Article *in* Physical Chemistry Chemical Physics · November 2017

DOI: 10.1039/C7CP05139E

CITATIONS
13

READS
86

3 authors:

Ol'ha O Brovarets
Institute of Molecular Biology and Genetics of NAS of Ukraine, Kyiv, Ukraine
307 PUBLICATIONS **2,082** CITATIONS
SEE PROFILE

Ivan S. Voiteshenko
National Taras Shevchenko University of Kyiv
33 PUBLICATIONS **58** CITATIONS
SEE PROFILE

Dmytro Mykolayovych Hovorun
National Academy of Sciences of Ukraine
615 PUBLICATIONS **3,921** CITATIONS
SEE PROFILE

PCCP

PAPER

Cite this: *Phys. Chem. Chem. Phys.*, 2018, **20**, 623

Physico-chemical profiles of the wobble ↔ Watson–Crick G*·2AP(w) ↔ G·2AP(WC) and A·2AP(w) ↔ A*·2AP(WC) tautomerisations: a QM/QTAIM comprehensive survey†

Ol'ha O. Brovarets',[ab] Ivan S. Voiteshenko[b] and Dmytro M. Hovorun[ab]

Received 29th July 2017,
Accepted 23rd November 2017

DOI: 10.1039/c7cp05139e

rsc.li/pccp

This study is intended to clarify in detail the tautomeric transformations of the wobble (w) G*·2AP(w) and A·2AP(w) nucleobase mispairs involving 2-aminopurine (2AP) into the Watson–Crick (WC) G·2AP(WC) and A*·2AP(WC) base mispairs (asterisks denote mutagenic tautomers of the DNA bases), respectively, by quantum-mechanical methods and Bader's Quantum Theory of Atoms in Molecules. Our previously reported methodology has been used, which allows the evolution of the physico-chemical parameters to be tracked along the entire internal reaction coordinate (IRC), not exclusively in the stationary states of these reactions. These biologically important G*·2AP(w) ↔ G·2AP(WC) and A·2AP(w) ↔ A*·2AP(WC) w ↔ WC tautomerisations, which are involved in mutagenic tautomerically-conformational pathways, determine the origin of the transitions and transversions induced by 2AP. In addition, it is established that they proceed through planar, highly stable, zwitterionic transition states and they exhibit similar physico-chemical profiles and stages of sequential intrapair proton transfer, followed by spatial rearrangement of the nucleobases relative to each other within the base pairs. These w ↔ WC tautomerisations occur non-dissociatively and are accompanied by a significant alteration in geometry (from wobble to Watson–Crick and *vice versa*) and redistribution of the specific intermolecular interactions, which can be divided into 10 patterns including AH···B H-bonds and loosened A–H–B covalent bridges along the IRC of tautomerisation. Based on the redistribution of the geometrical and electron-topological parameters of the intrapair hydrogen bonds, exactly 9 key points have been allocated to characterize the evolution of these reactions.

Introduction

Establishment of the fundamental mechanisms of the origin of point mutations induced by analogues of DNA bases is an intriguing topic in biophysics of DNA due to their importance in human health and numerous technical applications.[1–8]

To date, several experimental[9–22] and theoretical[23–26] studies have reported the mechanisms of action of the classic mutagen 2-aminopurine (2AP), which is also used as a fluorescent probe,[18–21] inducing A·T → G·C and G·C → A·T transitions.[11,12] However, these results are essentially independent and do not represent a complete picture of the mechanisms of the origin of the point mutations in DNA induced by 2AP.

In recent papers,[27–35] a solution of this extremely important and very difficult biological problem was comprehensively and thoroughly addressed by analyzing the structural mechanisms of the 2AP mutagenic pressure on DNA due to the latest breakthrough in the precise understanding of the origin of spontaneous point mutagenesis in DNA[36–42] within the framework of the classical Watson–Crick tautomeric hypothesis.[43]

Moreover, our theoretical data on spontaneous point mutations and that induced by analogues of the DNA bases, in particular transitions and transversions, are in good agreement with the experimental observations.[9–22,44–48]

In particular, our results prove that 2AP produces transversions by forming a wobble (w) mispair with A DNA base, A·2AP(w), followed by further A·2AP(w) → A*·2AP(WC) (WC – Watson–Crick) tautomerisation and subsequent A*·2AP(WC) → A*·2AP$_{syn}$ conformational transition, thus acquiring the A*·2AP$_{syn}$ enzymatically-competent conformation[33] (herein, the asterisk denotes the mutagenic tautomers of the DNA bases[49–57]).

[a] *Department of Molecular and Quantum Biophysics, Institute of Molecular Biology and Genetics, National Academy of Sciences of Ukraine, 150 Akademika Zabolotnoho Str., 03680 Kyiv, Ukraine. E-mail: o.o.brovarets@imbg.org.ua*

[b] *Department of Molecular Biotechnology and Bioinformatics, Institute of High Technologies, Taras Shevchenko National University of Kyiv, 2-h Akademika Hlushkova Ave., 03022 Kyiv, Ukraine*

† Electronic supplementary information (ESI) available: Profiles of the relative electronic energy along the IRC of the G*·2AP(w) ↔ G·2AP(WC) and A·2AP(w) ↔ A*·2AP(WC) w ↔ WC tautomerisations in the continuum with $\varepsilon = 4$, characteristic of the active center of the DNA-polymerase. See DOI: 10.1039/c7cp05139e

It was also shown for the first time that 2AP* may also produce another transversion when the 2AP* mutagenic tautomer pairs with the G base to form the G·2AP*(w) mispair, which converts to the G·2AP$_{syn}$ enzymatically-competent structure *via* consecutive tautomeric and conformational transformations: G·2AP*(w) → G*·2AP(w) → G·2AP(WC) → G·2AP$_{syn}$.[32] In this case, the long G·2AP(WC) WC-like mispair acts as a precursor to the enzymatically-competent conformation, the G·2AP$_{syn}$ mispair.

The estimated ratio of probabilities $P_{A\cdot 2AP}/P_{A\cdot A} = 40.5$[33] and $P_{G\cdot 2AP^*}/P_{G\cdot A^*} = 1.9 \times 10^7$ [32] indicates that these structural transformation routes are mutagenic. Notably, the formed A*·2AP$_{syn}$ and G·2AP$_{syn}$ base pairs quite easily acquire an enzymatically-competent WC conformation during the process of thermal fluctuations, which enables their successful incorporation into the DNA double helix by the high-fidelity replicative DNA-polymerase.

The present work presents a detailed quantum-mechanical/Quantum Theory of Atoms in Molecules (QM/QTAIM) investigation of the physico-chemical parameters at each point of the intrinsic reaction coordinate (IRC) of the acquisition by the G*·2AP(w) and A·2AP(w) nucleobase mispairs involving the 2AP mutagen[27–30] with Watson–Crick geometry due to the G*·2AP(w) ↔ G·2AP(WC) and A·2AP(w) ↔ A*·2AP(WC) w ↔ WC tautomerisations. This investigation enables the monitoring of the energetic, polar, geometric, charge, electron-topological and natural bond orbital (NBO) characteristics of the base mispairs and intrapair interactions along the IRC. It is worthy to note that the profiles of the geometric parameters, including the distance $R(H_9–H_9)$ between the H_9 and H_9 glycosidic hydrogens, glycosidic angles α_1/α_2, $d_{A\cdots B}$ distances between the electronegative A and B atoms, ∠AH···B angles of the AH···B hydrogen (H) bonds and patterns of the energy of the intermolecular H-bonds E_{HB} indicate significant rebuilding of the geometry of the nucleobase pairs and the non-dissociative character of these biologically important w ↔ WC tautomerisations, which occur without breakage of the pairs. Using the obtained evolutions of the physico-chemical parameters along the IRC, 9 key points (KPs) have been established, which allow the phases of the reactions to be distinguish and demonstrate that in the course of these w ↔ WC tautomerisations, protons move sequentially without a stable intermediate, followed by spatial rearrangement of the nucleobases relative to each other within the base pairs.

Computational methods

All calculations were performed using the Gaussian'09 program package.[58] The geometries and harmonic vibrational frequencies of the considered base mispairs and transition states (TSs) of their mutual tautomeric conversions were obtained in our previous work at the B3LYP/6-311++G(d,p) level of theory, which suggested that it is suitable for the investigation of similar systems,[59,60] followed by single point energy calculations at the MP2/aug-cc-pVDZ level of theory.[27–35]

In order to consider the surrounding effect on the investigated tautomerisation processes, we used the conductor-like polarizable continuum model (CPCM),[61,62] choosing the continuum with a dielectric constant $\varepsilon = 4$, which is typical for the active center of DNA-polymerase.[63,64]

The reaction pathway for the proton transfer (PT) tautomerisation of the wobble base mispairs was obtained by following the IRC in the forward and reverse directions from the transition state (TS) using the Hessian-based predictor–corrector integration algorithm[65] with tight convergence criteria. We obtained the profiles of the energetic, geometric, polar, charge, electron-topological and NBO characteristics of the H-bonds and complexes along the pathway of the tautomerisation reactions by calculating them at each point of the IRC using our previously reported methodology.[66–70] The profiles of the NBO charges along the IRC were obtained using the NBO program,[71] which was implemented in the Gaussian'09[58] program package.

Bader's quantum theory of atoms in molecules (QTAIM) was applied to analyse the electron density distribution[72] using the program package AIMAll[73] with all default options. The presence of a bond critical point (BCP), namely the so-called (3,−1) BCP, and a bond path between hydrogen donor and acceptor, as well as the positive value of the Laplacian at this BCP ($\Delta\rho > 0$), were considered as criteria for H-bond formation.[74] Wave functions were obtained at the level of theory used for geometry optimisation.

The H-bond energy, E_{HB}, was calculated using the empirical Espinosa–Molins–Lecomte (EML) formula[75,76] based on the electron density distribution at the (3,−1) BCPs of the H-bonds:

$$E_{HB} = 0.5 \cdot V(r)$$

where, $V(r)$ is the value of a local potential energy at the (3,−1) BCP.

The atomic numbering scheme for the nucleotide bases is conventional.[77]

Results and discussion

Exhaustive analysis of the potential energy surface

Comprehensive analysis of the potential energy surface and IRC calculations revealed that the G*·2AP(w) ↔ G·2AP(WC) and A·2AP(w) ↔ A*·2AP(WC) w ↔ WC tautomerisations occur *via* the initial transfer of the single proton localized at the O6/N6 atoms of the G*/A DNA bases in the wobble G*·2AP(w)/A·2AP(w) mispairs along the upper O6/N6H···N1 H-bonds to the 2AP base followed by the shifting of the 2AP base according the G*/A DNA bases into the minor groove of DNA. This results in the localized transition states $TS^{G^-\cdot 2AP^+}_{G^*\cdot 2AP(w)\leftrightarrow G\cdot 2AP(WC)}$/$TS^{A^-\cdot 2AP^+}_{A\cdot 2AP(w)\leftrightarrow A^*\cdot 2AP(WC)}$ since the $G^-/A^-\cdot 2AP^+$ tight ion pairs are stabilized by the participation of the network of the $C6^+H\cdots O6^-/N6^-$, $N1^+H\cdots O6^-/N6^-$, $N1^+H\cdots N1^-$, $N2^+H\cdots N1^-$, and $N2^+H\cdots N2^-$ H-bonds (Fig. 1 and 5) with the $\Delta\Delta G_{TS}/\Delta\Delta E_{TS}$ barriers of 18.04/16.58 and 29.85/31.00 kcal mol^{-1} (Tables 2–5), respectively. Further, the reagent complexes finally acquire the Watson–Crick geometry and the mobile proton at the N1 atom of the $2AP^+$ base moves

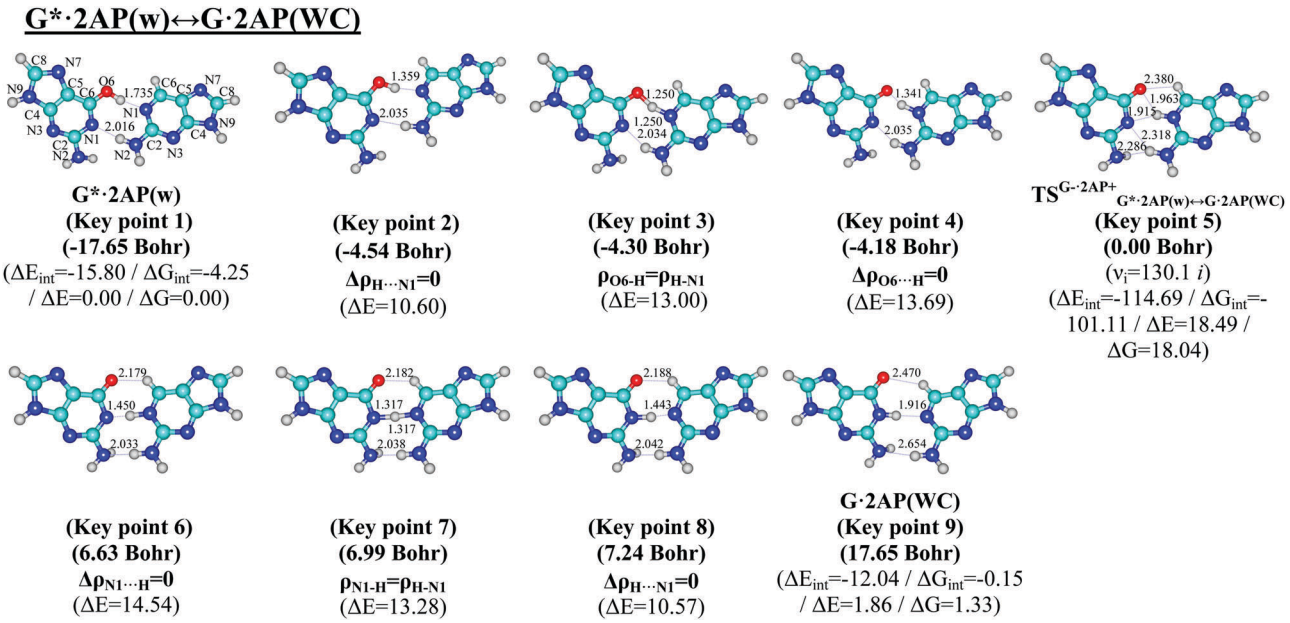

Fig. 1 Geometrical structures of the 9 key points describing the evolution of the G*·2AP(w) ↔ G·2AP(WC) w ↔ WC tautomerisation *via* the sequential PT along the IRC obtained at the B3LYP/6-311++G(d,p) level of theory *in vacuo*. The coordinates of the 9 key points, their relative Gibbs free energies ΔG or relative electronic energies ΔE (in kcal mol^{-1} obtained at the MP2/aug-cc-pVDZ//B3LYP/6-311++G(d,p) level of theory in the continuum with ε = 1 at T = 298.15 K) and imaginary frequencies ν_i (cm^{-1}) at the TSs of their interconversions are presented below them in brackets. The dotted lines indicate AH···B H-bonds, while the continuous lines show covalent bonds (their lengths are presented in angstroms). Carbon atoms are in light-blue, nitrogen in dark-blue, hydrogen in grey and oxygen in red.

back to the N1 atom of the G*/A DNA bases along the middle N1H···N1 H-bond. This compensates the excessive charge of the 2AP$^+$ nucleobase and leads to the formation of the G·2AP(WC)/A*·2AP(WC) Watson–Crick-like nucleobase mispairs joined by the C6H···O6/N6, N1H···N1, and N2/C2H···N2/HN2 H-bonds with relative $\Delta\Delta G/\Delta\Delta E$ energies of 1.33/1.07 and 13.71/13.57 kcal mol^{-1} (Table 1), respectively. It was established that for the minima, which are the initial G*·2AP(w)/A·2AP(w) and terminal G·2AP(WC)/A*·2AP(WC) complexes, all frequencies of the normal vibrations are real, whereas the TSs possess one imaginary frequency, corresponding to the shifting motion of the bases relative to each other into the minor and major DNA grooves.

Analysis of the potential energy surface shows that these reactions proceed through the sequential intrapair PT.

The profiles of the electronic energy of the G*·2AP(w) ↔ G·2AP(WC) and A·2AP(w) ↔ A*·2AP(WC) tautomerisation reactions are quite smooth in the vicinity of the TSs. In contrast,

Table 1 Energetic and kinetic characteristics of the biologically important tautomerisations of the investigated mispairs containing purine canonical DNA bases and 2-aminopurine nucleobase in the main or rare tautomeric forms leading to incorporation and replication errors (MP2/aug-cc-pVDZ//B3LYP/6-311++G(d,p) level of theory in the continuum with ε = 1 and ε = 4) (see also Fig. S1, ESI)

Tautomeric transformation	ν_i[a]	ΔG[b]	ΔE[c]	$\Delta\Delta G_{TS}$[d]	$\Delta\Delta E_{TS}$[e]	$\Delta\Delta G$[f]	$\Delta\Delta E$[g]	k_f[h]	k_r[i]	$\tau_{99.9\%}$[j]	τ[k]
ε = 1											
G*·2AP(w) ↔ G·2AP(WC)	130.1	1.33	1.07	18.04	16.58	16.70	15.51	0.37	3.53	1.77	0.28
G*·A(w) ↔ G·A(WC)	107.2	−4.30	−6.73	12.33	9.97	16.64	16.70	5.64×10^{3}	3.94	1.22×10^{-3}	0.25
A·2AP(w) ↔ A*·2AP(WC)	117.0	13.71	13.57	29.85	31.00	16.14	17.43	8.01×10^{-10}	9.10	0.76	0.11
A·A(w) ↔ A*·A(WC)	152.4	3.63	1.09	25.86	22.56	22.24	21.47	6.79×10^{-7}	3.10×10^{-4}	2.22×10^{4}	3.22×10^{3}
ε = 4											
G*·2AP(w) ↔ G·2AP(WC)	104.6	−1.20	−1.09	12.30	11.61	13.50	12.71	5.93×10^{3}	7.80×10^{2}	1.03×10^{-3}	1.28×10^{-3}
G*·A(w) ↔ G·A(WC)	84.5	−4.87	−6.90	8.42	6.08	13.29	12.98	4.20×10^{6}	1.11×10^{3}	8.97×10^{-4}	1.65×10^{-6}
A·2AP(w) ↔ A*·2AP(WC)	95.9	12.62	11.88	26.53	26.33	13.91	14.45	2.18×10^{-7}	3.95×10^{2}	1.75×10^{-2}	2.53×10^{-3}
A·A(w) ↔ A*·A(WC)	108.3	6.82	2.37	21.82	19.19	15.01	16.82	6.17×10^{-4}	61.71	0.11	1.62×10^{-2}

Note: [a] Imaginary frequency at the TSs of the tautomerisation reaction, cm^{-1}. [b] The Gibbs free energy of the product relative to the reactant of the tautomerisation reaction (T = 298.15 K), kcal mol^{-1}. [c] The electronic energy of the product relative to the reactant of the tautomerisation reaction, kcal mol^{-1}. [d] The Gibbs free energy barrier for the forward reaction of tautomerisation, kcal mol^{-1}. [e] The electronic energy barrier for the forward reaction of the tautomerisation, kcal mol^{-1}. [f] The Gibbs free energy barrier for the reverse reaction of the tautomerisation, kcal mol^{-1}. [g] The electronic energy barrier for the reverse reaction of the tautomerisation, kcal mol^{-1}. [h] The forward rate constant for the tautomerisation reaction, s^{-1}. [i] The reverse rate constant for the tautomerisation reaction, s^{-1}. [j] The time necessary to reach 99.9% of the equilibrium concentration between the reactant and the product of the tautomerization reaction, s. [k] The lifetime of the product of the tautomerisation reaction, s.

Table 2 Electron-topological and structural characteristics of the specific intermolecular bonds revealed in the 9 key points and the polarity of the latter along the IRC of the G*·2AP(w) ↔ G·2AP(WC) tautomerisation obtained at the B3LYP/6-311++G(d,p) level of theory in the continuum with ε = 1

Complex	AH···B H-bond/A–H/H–B covalent bond	ρ^a	$\Delta\rho^b$	$100{\cdot}\varepsilon^c$	$d_{A\cdots B}{}^d$	$d_{H\cdots B}{}^e$	∠AH···B^f	μ^g
Key point 1 (−17.65 Bohr): G*·2AP(w)	O6H···N1	0.049	0.100	5.14	2.728	1.735	168.4	4.58
	N1···HN2	0.026	0.077	7.43	3.029	2.016	171.3	
Key point 2 (−4.54 Bohr): $\Delta\rho_{H\cdots N1}$ = 0	O6H···N1	0.126	−0.037	3.27	2.492	1.359	164.3	5.64
	N1···HN2	0.025	0.076	6.60	2.989	2.035	155.0	
Key point 3 (−4.30 Bohr): $\rho_{O6-H} = \rho_{H-N1}$	O6–H/H–N1	0.169	−0.317	2.79	2.500	1.250	161.9	6.82
	N1···HN2	0.025	0.075	6.65	2.989	2.034	154.8	
Key point 4 (−4.18 Bohr): $\Delta\rho_{O6\cdots H}$ = 0	O6···HN1	0.124	0.008	2.25	2.507	1.341	160.5	7.41
	N1···HN2	0.025	0.074	6.64	2.990	2.035	154.6	
Key point 5 (0.00 Bohr): $TS^{G^-\cdot 2AP^+}_{G^*\cdot 2AP(w)\leftrightarrow G\cdot 2AP(WC)}$	$O6^-\cdots HC6^+$	0.013	0.049	67.40	2.961	2.380	112.0	10.62
	$O6^-\cdots HN1^+$	0.028	0.092	26.10	2.754	1.963	129.7	
	$N1^-\cdots HN1^+$	0.031	0.088	6.86	2.910	1.915	156.9	
	$N1^-\cdots HN2^+$	0.014	0.045	8.67	3.166	2.318	139.9	
	$N2^-\cdots HN2^+$	0.013	0.044	9.18	3.240	2.286	155.5	
Key point 6 (6.63 Bohr): $\Delta\rho_{N1\cdots H}$ = 0	O6···HC6	0.018	0.064	7.54	2.963	2.179	127.1	9.50
	N1···HN1	0.104	0.006	4.74	2.628	1.450	173.5	
	N2···HN2	0.025	0.072	5.73	3.039	2.033	167.3	
Key point 7 (6.99 Bohr): $\rho_{N1-H} = \rho_{H-N1}$	O6···HC6	0.018	0.064	7.52	2.965	2.182	127.0	8.47
	N1–H/H–N1	0.145	−0.168	3.56	2.612	1.317	172.4	
	N2···HN2	0.025	0.073	6.23	3.038	2.038	166.5	
Key point 8 (7.24 Bohr): $\Delta\rho_{H\cdots N1}$ = 0	O6···HC6	0.017	0.063	7.64	2.967	2.188	126.7	7.79
	N1H···N1	0.105	0.024	4.32	2.610	1.443	170.9	
	N2···HN2	0.025	0.074	6.51	3.039	2.042	166.3	
Key point 9 (17.65 Bohr): G·2AP(WC)	O6···HC6	0.010	0.029	2.90	3.366	2.470	138.9	7.72
	N1H···N1	0.033	0.088	6.76	2.948	1.916	176.2	
	N2···HN2	0.008	0.026	110.77	3.400	2.654	130.7	

Notes: ^{a} The electron density at the (3,−1) BCP, a.u. ^{b} The Laplacian of the electron density at the (3,−1) BCP, a.u. ^{c} The ellipticity at the (3,−1) BCP. ^{d} The distance between the A (H-bond donor) and B (H-bond acceptor) atoms of the AH···B H-bonds, Å. ^{e} The distance between the H and B atoms of the AH···B H-bonds, Å. ^{f} The H-bond angle, degree. ^{g} The dipole moment of the complex, D.

Table 3 Patterns of the specific intermolecular interactions including AH···B H-bonds and loosened A–H–B covalent bridges that sequentially replace each other along the IRC of the G*·2AP(w) ↔ G·2AP(WC) w ↔ WC tautomerisation *via* the sequential PT obtained at the B3LYP/6-311++G(d,p) level of theory in the continuum with ε = 1

Patterns	IRC range, Bohr	Specific intermolecular interactions, forming patterns
I	[−17.65 to −4.54)	(G)O6H···N1(2AP), (G)N1···HN2(2AP)
II	[−4.54 to −4.18)	(G)O6-H-N1(2AP), (G)N1···HN2(2AP)
III	[−4.18 to −2.46)	(G)O6···HN1(2AP), (G)N1···HN2(2AP)
IV	[−2.46 to −1.97)	(G)O6···HN1(2AP), (G)N1···HN2(2AP), (G)N2···HN2(2AP)
V	[−1.97 to −0.86)	(G)O6···HN1(2AP), (G)N1···HN1(2AP), (G)N1···HN2(2AP), (G)N2···HN2(2AP)
VI	[−0.86 to 2.21)	(G)O6···HC6(2AP), (G)O6···HN1(2AP), (G)N1···HN1(2AP), (G)N1···HN2(2AP), (G)N2···HN2(2AP)
VII	[2.21 to 3.56)	(G)O6···HC6(2AP), (G)N1···HN1(2AP), (G)N1···HN2(2AP), (G)N2···HN2(2AP)
VIII	[3.56 to 6.75)	(G)O6···HC6(2AP), (G)N1···HN1(2AP), (G)N2···HN2(2AP)
IX	[6.75 to 7.24)	(G)O6···HC6(2AP), (G)N1-H-N1(2AP), (G)N2···HN2(2AP)
X	[7.24 to 17.65]	(G)O6···HC6(2AP), (G)N1H···N1(2AP), (G)N2···HN2(2AP)

peaks and fractures are present on both sides of the TSs, which correspond to the range of existence of the $G^-/A^-\cdot 2AP^+$ ion pairs during their transformations, namely to KP 4 and KP 6 (Fig. 2a and 6a, respectively).

The transition from vacuum to weakly polar continuum with ε = 4, which is typical for the interfaces of specific protein–nucleic acid interactions, does not qualitatively affect the course and structure of the transition state of the tautomerisation reactions (Fig. S1, ESI†). This could be explained by the fact that this transition does not disturb the structure of the TSs of these tautomerisations, since it is a highly stable, tight ion pair. Simultaneously, this transition accelerates the w ↔ WC tautomerisation, while the shape of the curves dependent on the energy of the studied pairs from the IRC does not significantly change (Fig. S1, ESI†).

The calculated first derivatives of the electronic energy E by the IRC, in particular, the peaks on its curve, enable the reaction pathways of these reactions to be divided into regions of reagent (13.11/13.17 Bohr), transition state (11.78/9.81 Bohr) and product (10.41/11.71 Bohr) based on the data collected by us[31–37] and our colleagues[78–80] (Fig. 2b and 6b). The widest is the preparation reagent stage corresponding to the intrapair proton transfer, whereas the narrowest is the TS region, where mutual reorientation and shifting of the bases relative to each other occur. Consequently, the direct initiation of the G*·2AP(w) → G·2AP(WC) and A·2AP(w) → A*·2AP(WC) reactions requires the electronic energy $\Delta E_{KP2} - \Delta E_{KP1[G^*\cdot 2AP(w)/A\cdot 2AP(w)]}$ = 10.60/18.75 kcal mol^{-1}, which represents 57.3%/56.4% of the electronic energies of the TSs. In contrast, much less energy is required for the final

Table 4 Electron-topological and structural characteristics of the specific intermolecular bonds revealed in the 9 key points and the polarity of the latter along the IRC of the A·2AP(w) ↔ A*·2AP(WC) tautomerisation obtained at the B3LYP/6-311++G(d,p) level of theory in the continuum with ε = 1

Complex	AH···B H-bond/A–H/H–B covalent bond	ρ	$\Delta\rho$	$100{\cdot}\varepsilon$	$d_{A\cdots B}$	$d_{H\cdots B}$	$\angle$AH···B	μ
Key point 1 (−18.38 Bohr): A·2AP(w)	N6H···N1	0.029	0.081	7.56	3.002	1.976	179.4	1.09
	N1···HN2	0.026	0.076	7.89	3.043	2.021	179.7	
Key point 2 (−5.21 Bohr): $\Delta\rho_{H\cdots N1}$ = 0	N6H···N1	0.105	0.033	3.41	2.598	1.426	171.9	3.37
	N1···HN2	0.028	0.083	7.18	2.957	1.977	159.5	
Key point 3 (−4.96 Bohr): ρ_{N6-H} = ρ_{H-N1}	N6–H/H–N1	0.142	−0.146	2.79	2.602	1.313	168.7	4.91
	N1···HN2	0.029	0.082	7.20	2.957	1.974	159.5	
Key point 4 (−4.60 Bohr): $\Delta\rho_{N6\cdots H}$ = 0	N6···HN1	0.098	0.011	4.80	2.621	1.475	163.0	7.06
	N1···HN2	0.029	0.080	7.18	2.959	1.974	159.2	
Key point 5 (0.00 Bohr): $TS^{A-\cdot 2AP+}_{A\cdot 2AP(w)\leftrightarrow A^{*}\cdot 2AP(WC)}$	$N6^{-}\cdots HC6^{+}$	0.016	0.052	9.19	3.023	2.344	119.0	9.98
	$N6^{-}\cdots HN1^{+}$	0.020	0.071	47.64	2.887	2.131	126.4	
	$N1^{-}\cdots HN1^{+}$	0.039	0.089	1.05	2.860	1.834	162.3	
	$N1^{-}\cdots HN2^{+}$	0.015	0.048	4.15	3.154	2.277	144.0	
Key point 6 (4.00 Bohr): $\Delta\rho_{N1\cdots H}$ = 0	N6···HC6	0.020	0.063	1.63	3.012	2.205	129.1	8.54
	N1···HN1	0.097	0.016	4.34	2.661	1.482	179.2	
	C2H···HN2	0.008	0.029	25.88	2.689	2.049	114.3	
Key point 7 (4.35 Bohr): ρ_{N1-H} = ρ_{H-N1}	N6···HC6	0.020	0.063	1.55	3.014	2.209	129.0	6.98
	N1–H/H–N1	0.145	−0.181	3.36	2.645	1.317	177.8	
Key point 7 (4.60 Bohr): $\Delta\rho_{H\cdots N1}$ = 0	C2H···HN2	0.008	0.028	18.64	2.701	2.051	115.2	
Key point 8 (4.60 Bohr): $\Delta\rho_{H\cdots N1}$ = 0	N6···HC6	0.019	0.063	1.45	3.015	2.215	128.6	5.79
	N1H···N1	0.106	0.012	4.02	2.642	1.440	176.2	
	C2H···HN2	0.008	0.028	15.70	2.704	2.052	115.4	
Key point 9 (16.31 Bohr): A*·2AP(WC)	N6···HC6	0.013	0.039	5.58	3.332	2.388	144.2	4.55
	N1H···N1	0.029	0.082	7.01	2.991	1.961	175.2	
	C2H···HN2	0.001	0.005	75.42	3.668	2.987	125.7	

Notes: for footnote definitions see Table 2.

Table 5 Patterns of the specific intermolecular interactions including AH···B H-bonds and loosened A–H–B covalent bridges that sequentially replace each other along the IRC of the A·2AP(w) ↔ A*·2AP(WC) w ↔ WC tautomerisation *via* the sequential PT obtained at the B3LYP/6-311++G(d,p) level of theory in the continuum with ε = 1

Patterns	IRC range, Bohr	Specific intermolecular interactions, forming patterns
I	[−18.34 to −5.09)	(A)N6H···N1(2AP), (A)N1···HN2(2AP)
II	[−5.09 to −4.60)	(A)N6–H–N1(2AP), (A)N1···HN2(2AP)
III	[−4.60 to −3.51)	(A)N6···HN1(2AP), (A)N1···HN2(2AP)
IV	[−3.51 to −2.91)	(A)N6···HN1(2AP), (A)N1···HN1(2AP), (A)N1·····HN2(2AP)
V	[−2.91 to 1.21)	(A)N6···HC6(2AP), (A)N6···HN1(2AP), (A)N1···HN1(2AP), (A)N1···HN2(2AP)
VI	[1.21 to 2.30)	(A)N6···HC6(2AP), (A)N1···HN1(2AP), (A)N1···HN2(2AP)
VII	[2.30 to 3.26)	(A)N6···HC6(2AP), (A)N1···HN1(2AP), (A)N1···HN2(2AP), (A)C2H···HN2(2AP)
VIII	[3.26 to 4.23)	(A)N6···HC6(2AP), (A)N1···HN1(2AP), (A)C2H···HN2(2AP)
IX	[4.23 to 4.60)	(A)N6···HC6(2AP), (A)N1–H–N1(2AP), (A)C2H···HN2(2AP)
X	[4.60 to 16.31]	(A)N6···HC6(2AP), (A)N1H···N1(2AP), (A)C2H···HN2(2AP)

relaxation of the reaction complexes to the terminal mispairs: $\Delta E_{KP8} - \Delta E_{KP9[G\cdot 2AP(WC)/A^{*}\cdot 2AP(WC)]}$ = 8.71/13.85 kcal mol^{-1}, which represents 47.1%/41.4% of the energies of $TS^{G-\cdot 2AP+}_{G^{*}\cdot 2AP(w)\leftrightarrow G\cdot 2AP(WC)}$/$TS^{A-\cdot 2AP+}_{A\cdot 2AP(w)\leftrightarrow A^{*}\cdot 2AP(WC)}$. These observations indicate that more energy is required to initiate the reaction due to the preparatory PT before the structurally-electronic rebuilding of the nucleobases within the mispairs in the TS region, especially in the case of the A·2AP(w) → A*·2AP(WC) w → WC tautomerisation (~2 times), than for the final relaxation to the terminal mispairs (Fig. 2b).

The established data show the resemblance between the courses of these processes and their electronic energy profiles regardless of their structural difference (Fig. 1, 2, 5 and 6). Notably, these conversions with the participation of the 2AP analogue are established to be the same as that with the participation of the canonical A DNA bases G*·A(w) ↔ G·A(WC)[41] and A·A(w) ↔ A*·A(WC)[42] (Table 1).

Polar and charge characteristics

The profiles of the dipole moment reflecting the changes in the polarities along the IRC are bell-shaped near the TS (4.40–10.67/1.04–10.00 D) and almost plateau on each side of it with average values of 4.56/1.11 D on the left and 7.43/4.75 D on the right (Fig. 2c and 6c), respectively.

The calculated profiles of the NBO charges (0.402–0.508/0.375–0.493 *e*) of the hydrogen atoms involved in the intermolecular H-bonds are dome-shaped in the TS region with fractures, whereas they are almost constant lines at the beginning and ending of these tautomerisation reactions (Fig. 2d and 6d, respectively). The notable feature of the A·2AP(w) ↔ A*·2AP(WC) w ↔ WC tautomerisation is that the NBO charges for the H atoms located at the N2 and N6 atoms coincide at the beginning of the reaction (0.435 and 0.434 e), while their difference increases at the ending of the reaction (0.384 and 0.451 e) (Fig. 2d and 6d), respectively.

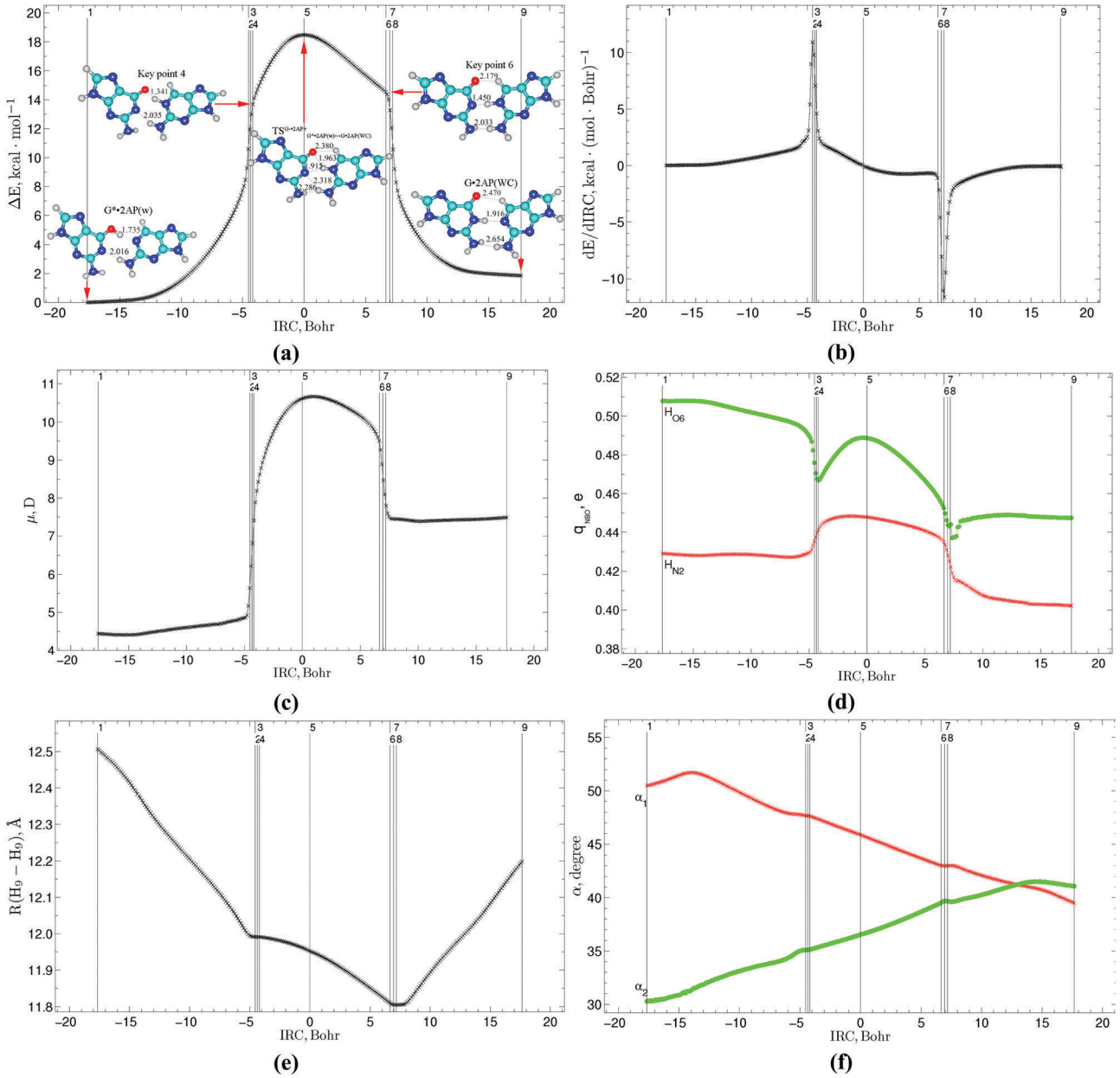

Fig. 2 Profiles of (a) relative electronic energy ΔE together with the stationary states (G*·2AP(w), $TS^{G-\cdot 2AP+}_{G^*\cdot 2AP(w)\leftrightarrow G\cdot 2AP(WC)}$, G·2AP(WC)) and KPs 4 and 6, (b) first derivative of the electronic energy with respect to the IRC (dE/dIRC), (c) dipole moment μ, (d) NBO charges q_{NBO}, (e) distance $R(H_9-H_9)$ between the H_9 and H_9 glycosidic hydrogens and (f) α_1 ($\angle$ N9H_9(2AP)H_9(G)) and α_2 ($\angle$ N9H_9(G)H_9(2AP)) glycosidic angles along the IRC of the G*·2AP(w) ↔ G·2AP(WC) w ↔ WC tautomerisation *via* the sequential PT obtained at the B3LYP/6-311++G(d,p) level of theory in the continuum with ε = 1.

Geometric and electron-topological characteristics of the mispairs and intermolecular H-bonds

Using our previously reported methodology[81–85] we calculated the changes in the main physico-chemical characteristics at each point of the IRC, which are presented in Fig. 2–4 and 6–8, respectively.

Based on the evolution of the geometrical parameters ($R(H_9–H_9)$, $d_{AH/HB}$ and $d_{A\cdots B}$ distances, α_1/α_2 and $\angle$AH$\cdots$B angles) along the IRC, it was found that the investigated reactions are followed by significant geometry changes in the base pairs, thus reflecting the large-scale movement of the bases relative to each other within the mispairs (Fig. 2e, f, 3d–f, 6e, f and 7d–f). The distinguished feature of the profiles of the glycosidic distances $R(H_9–H_9)$ (11.805–12.506/12.142–12.766 Å), distances between the hydrogen and electronegative atoms $d_{AH/HB}$ (1.004–3.353/1.003–3.696 Å), distances between the electronegative atoms $d_{A\cdots B}$ (2.490–4.023/2.597–4.209 Å) and angles of the H-bonding $\angle$AH$\cdots$B (89.4–173.9/89.0–179.7°) is the presence of kinks in the vicinity of the 2nd and 8th key points, which could be associated with the structural changes in the base mispairs from the wobble to the Watson–Crick architecture due to the

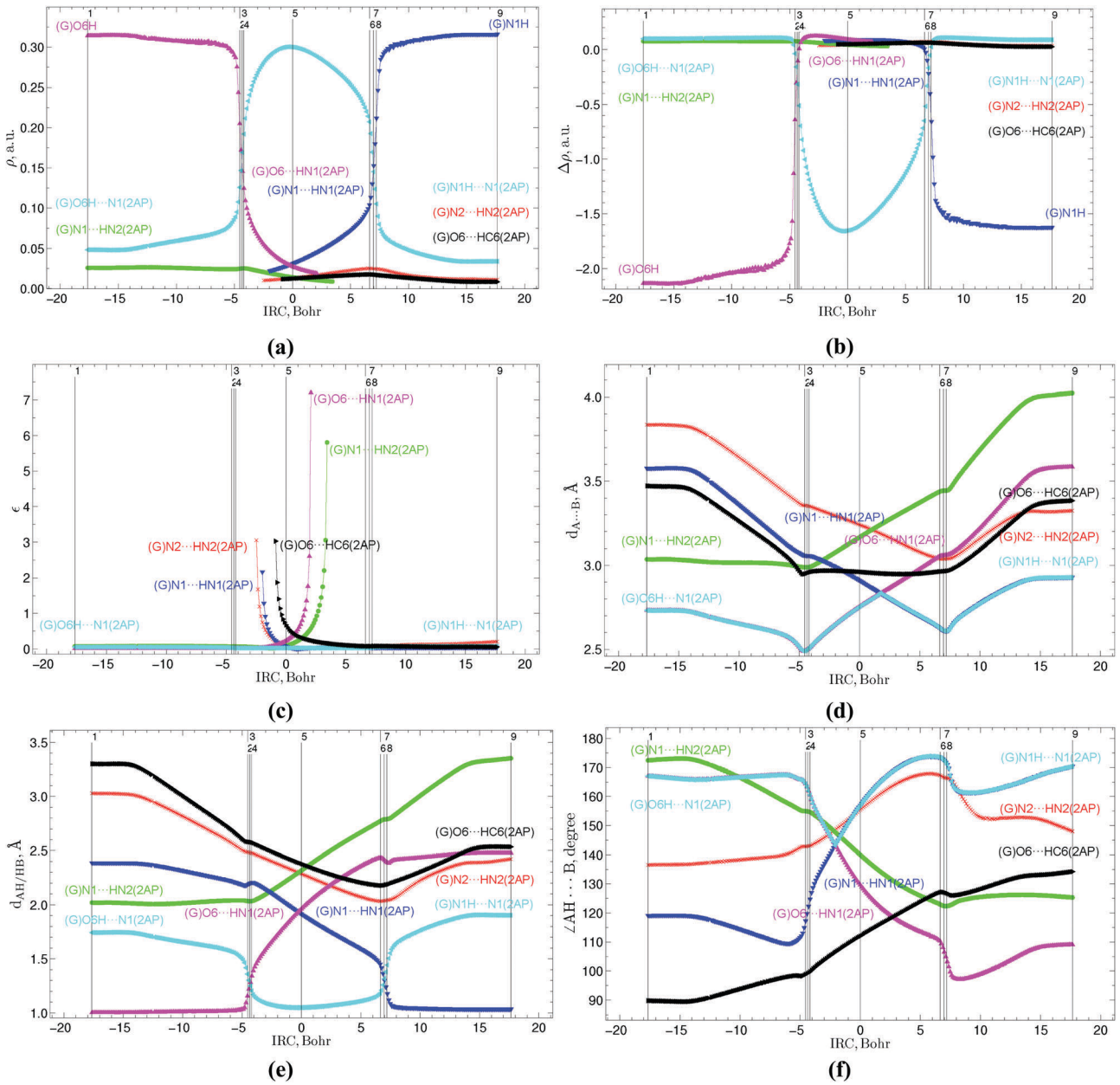

Fig. 3 Profiles of (a) electron density ρ; (b) Laplacian of the electron density $\Delta\rho$, (c) ellipticity ε at the (3,−1) BCPs, (d) distance $d_{A\cdots B}$ between the electronegative A and B atoms; (e) distance $d_{AH/HB}$ between the hydrogen and electronegative A or B atoms and (f) angle $\angle$AH···B of the H-bonds along the IRC of the G*·2AP(w) ↔ G·2AP(WC) w ↔ WC tautomerisation *via* the sequential PT obtained at the B3LYP/6-311++G(d,p) level of theory in the continuum with ε = 1.

shifting of the 2AP base downwards into the minor DNA groove according the G*/A bases. The same tendencies have also been observed for the 2AP·T(WC) ↔ 2AP·T*(w) and 2AP·C*(WC) ↔ 2AP·C(w) WC ↔ w tautomeric transformations.[34]

The curves of the α_1 glycosidic angle of 2AP gradually decrease, whereas the curves of the α_2 glycosidic angle of the G*/A bases gradually increase along the IRC, which vary in a broad range of values (30.3–51.7/31.7–53.3°) and equalize (41.2/39.7°) at IRC = 13.11/8.57 Bohr (Fig. 2f and 6f, respectively).

The calculations of the profiles of the electron-topological parameters at each point of the IRC, namely the electron density ρ (0.009–0.316/0.001–0.322 a.u.) and Laplacian of the electron density $\Delta\rho$ (−2.141–0.124/−1.703–0.127 a.u.), as well as the $d_{AH/HB}$ distances reveal their crossings at the transformations of the H-bonds along the IRC: (G/A)O6/N6H···N1(2AP) → (G/A)O6/N6···HN1(2AP) and (G/A)N1···HN1(2AP) → (G/A)N1H···N1(2AP) (Fig. 3a, b, e, 7a, b and e). These data correspond to the maximal and minimal values of ρ (0.169/0.142 and 0.145/0.145 a.u.), $\Delta\rho$ (−0.317/−0.146 and −0.168/−0.181 a.u.) and $d_{AH/HB}$ (1.250/1.313 and 1.317/1.317 Å) and enable the 2 key points containing loosened O6/N6–H–N1 and N1–H–N1 covalent bridges to be distinguished (Fig. 1 and 5), respectively, which are the 3rd (−4.30/−4.96 Bohr)

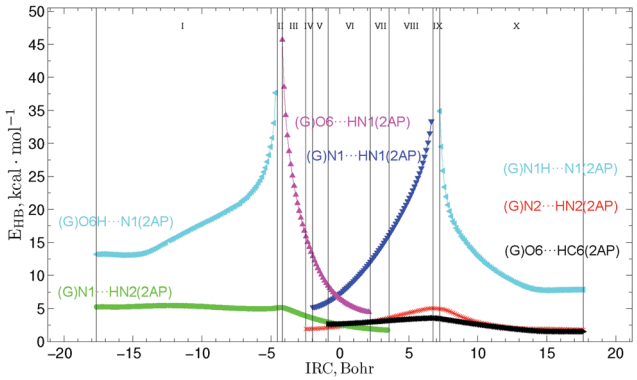

Fig. 4 Profiles of the energy of the intermolecular H-bonds E_{HB} estimated by the EML formula at the (3,−1) BCPs along the IRC of the G*·2AP(w) ↔ G·2AP(WC) w ↔ WC tautomerisation *via* the sequential PT obtained at the B3LYP/6-311++G(d,p) level of theory in the continuum with ε = 1 (see Table 3).

and 7th (6.99/4.35 Bohr) key points. Another 4 key points have been allocated as that where the Laplacian of the electron density $\Delta\rho$ equals zero, that is the H-bond converts to a covalent bond and *vice versa*, which are the 2nd (−4.54/−5.21 Bohr), 4th (−4.18/−4.60 Bohr), 6th (6.63/4.00 Bohr) and 8th (7.24/4.60 Bohr) key points. The other 3 key points, the 1st, 5th and 9th, represent stationary structures of the initial wobble G*·2AP(w)/A·2AP(w) base mispairs, the $TS^{G\cdots 2AP^{+}}_{G^{*}\cdot 2AP(w)\leftrightarrow G\cdot 2AP(WC)}$/$TS^{A\cdots 2AP^{+}}_{A\cdot 2AP(w)\leftrightarrow A^{*}\cdot 2AP(WC)}$ transition states and terminal Watson–Crick-like G·2AP(WC)/A*·2AP(WC) base mispairs (Fig. 1 and 5) respectively.

The profiles of the ellipticity ε at the (3,−1) BCPs of the (G/A)N1···HN2(2AP), (G/A)O6/N6···HC6(2AP), (G/A)N2/C2H···N2/HN2(2AP) intermolecular H-bonds gradually increase or decrease along the IRC, rapidly reaching their maxima on the borders, whereas the (G/A)O6/N6H···N1(2AP) and (G/A)N1H···N1(2AP) H-bonds remain almost stable along the IRC (Fig. 3c and 7c, respectively).

Similarly to the previously investigated 2AP·T(WC) ↔ 2AP·T*(w) and 2AP·C*(WC) ↔ 2AP·C(w) WC ↔ w tautomeric transformations,[34] the calculated evolutions of the energies E_{HB} of the intermolecular H-bonds could be divided into 10 patterns which sequentially change each other along the IRC (Tables 3, 5 and Fig. 4, 8).

The G*·2AP(w) ↔ G·2AP(WC) and A·2AP(w) ↔ A*·2AP(WC) w ↔ WC tautomerisations are accompanied by the formation and breakage of the intermolecular H-bonds, including simultaneously maximum 5 H-bonds in the first case, (G)O6···HC6(2AP), (G)O6···HN1(2AP), (G)N1···HN1(2AP), (G)N1···HN2(2AP) and (G)N2···HN2(2AP), within the ranges of IRC −0.86 to 2.21 Bohr and 4 H-bonds in the second case, (A)N6···HC6(2AP), (A)N6···HN1(2AP), (A)N1···HN1(2AP) and (A)N1···HN2(2AP) and (A)N6···HC6(2AP), (A)N1···HN1(2AP), (A)N1···HN2(2AP) and (A)C2H···HN2(2AP), within the ranges of IRC from −2.91 to 1.21 and from 2.30 to 3.26 Bohr, respectively. The curves of the (G/A)O6/N6H···N1(2AP) and (G/A)N1···HN1(2AP) H-bonds gradually increase from 13.19/6.10 to 37.64/36.11 and from 5.22/4.29 to 33.36/33.74 kcal mol^{-1}, curves of the (G/A)O6/N6···HN1(2AP) and (G/A)N1H···N1(2AP) H-bonds gradually decrease from 45.66/30.37 to 4.47/3.57 and from 34.90/36.64 to 7.86/6.11 kcal mol^{-1}, while the profiles of the (G/A)N1···HN2(2AP), (G/A)O6/N6H···N1(2AP) and (G/A)N2/C2H···HN2(2AP) H-bonds monotonically change along the IRC reaching their maximal values at the borders of the II and III (5.47/6.25 kcal mol^{-1}), VIII and IX (3.56/3.58 kcal mol^{-1}), and IX

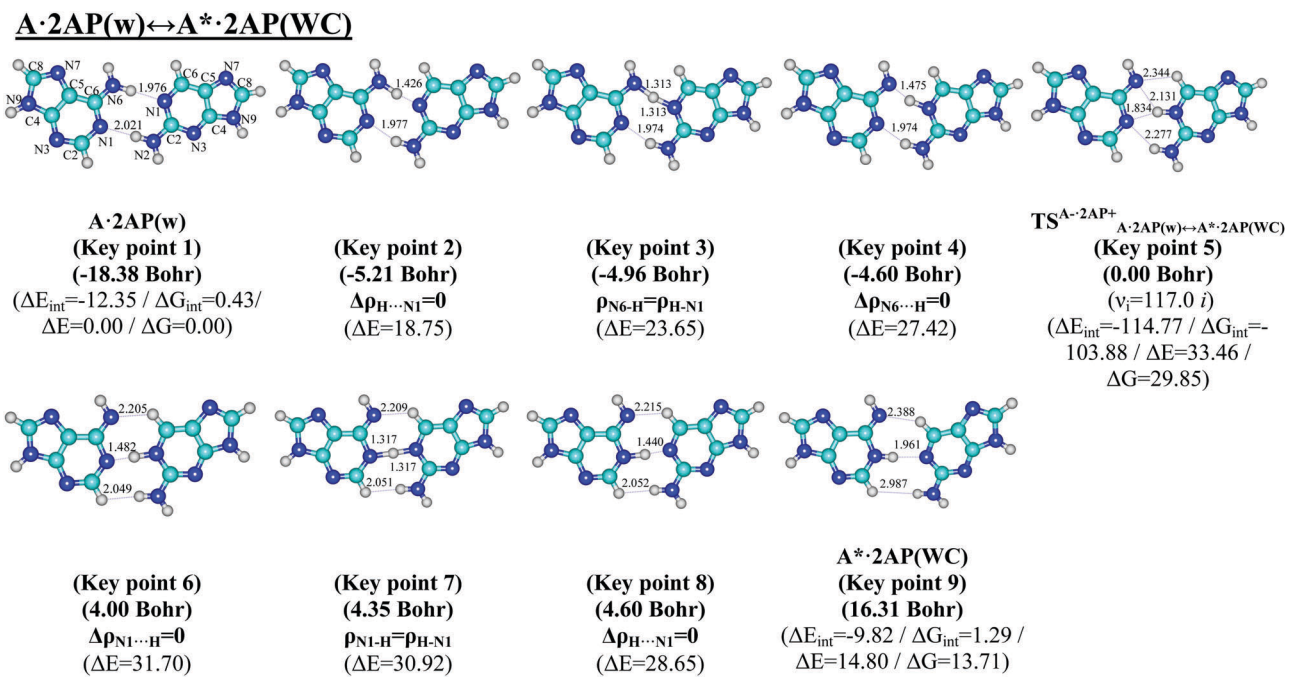

Fig. 5 Geometric structures of the 9 key points describing the evolution of the A·2AP(w) ↔ A*·2AP(WC) w ↔ WC tautomerisation *via* the sequential PT along the IRC obtained at the B3LYP/6-311++G(d,p) level of theory in the continuum with ε = 1. For designations see Fig. 1.

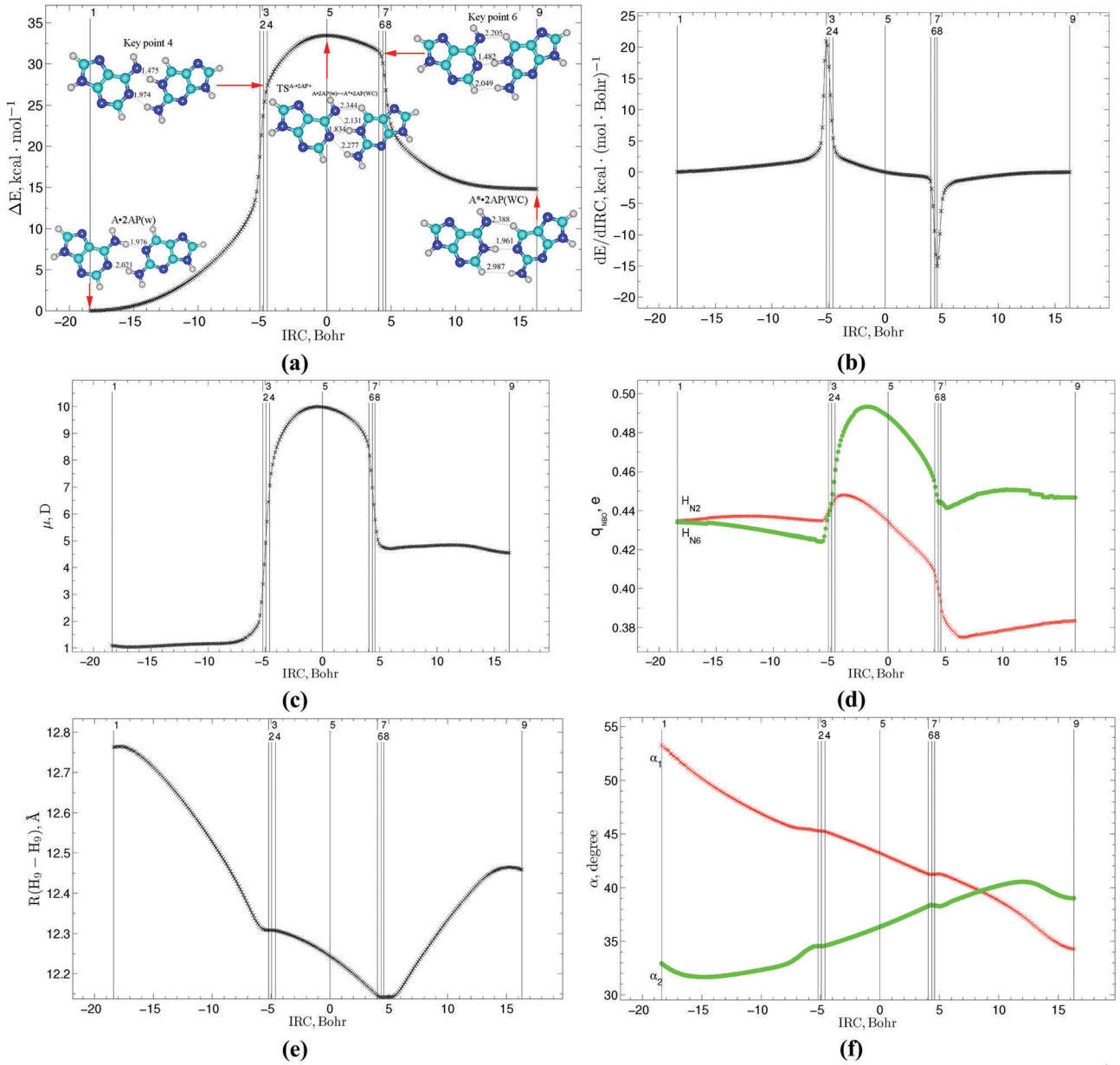

Fig. 6 Profiles of (a) relative electronic energy ΔE together with stationary states (A·2AP(w), $TS^{A^{-}\cdot 2AP^{+}}_{A\cdot 2AP(w)\leftrightarrow A^{*}\cdot 2AP(WC)}$, A*·2AP(WC)) and KPs 4 and 6, (b) first derivative of the electronic energy with respect to the IRC (dE/dIRC), (c) dipole moment μ, (d) NBO charges q_{NBO}, (e) distance $R(H_9–H_9)$ between the H_9 and H_9 glycosidic hydrogens and (f) α_1 (∠ $N9H_9(2AP)H_9(A)$) and α_2 (∠ $N9H_9(A)H_9(2AP)$) glycosidic angles along the IRC of the A·2AP(w) ↔ A*·2AP(WC) w ↔ WC tautomerisation *via* the sequential PT obtained at the B3LYP/6-311++G(d,p) level of theory in the continuum with ε = 1.

and X regions (5.04/1.36 kcal mol^{-1}) (Fig. 4 and 8, Tables 3 and 5).

It is worth mentioning that at the beginning of the A·2AP(w) ↔ A*·2AP(WC) reaction, the geometrical, energetic and electron-topological parameters almost coincide, that demonstrates their close values (Fig. 3, 4, 7 and 8, and Tables 2 and 4).

Close comparison of the obtained profiles for the w ↔ WC tautomeric conversions with the participation of the 2AP nucleobase analogue (Fig. 2–4, 6–8 and Fig. S1, ESI†) and canonical DNA bases[40,41] reflects high similarity between the courses of these processes and their scanning along the IRC. This represents an especially valuable observation since it could be used for the extension of the data for the canonical conversions to that with the participation of 2AP.

Notably, in all considered tautomerisation reactions, we did not fix the non-planar deformations of the DNA bases, despite their susceptibility to such processes.[86–88]

Conclusions

The current study is intended to give insight into the physico-chemical mechanism of the G*·2AP(w) ↔ G·2AP(WC) and A·2AP(w) ↔ A*·2AP(WC) w ↔ WC tautomerisations, which

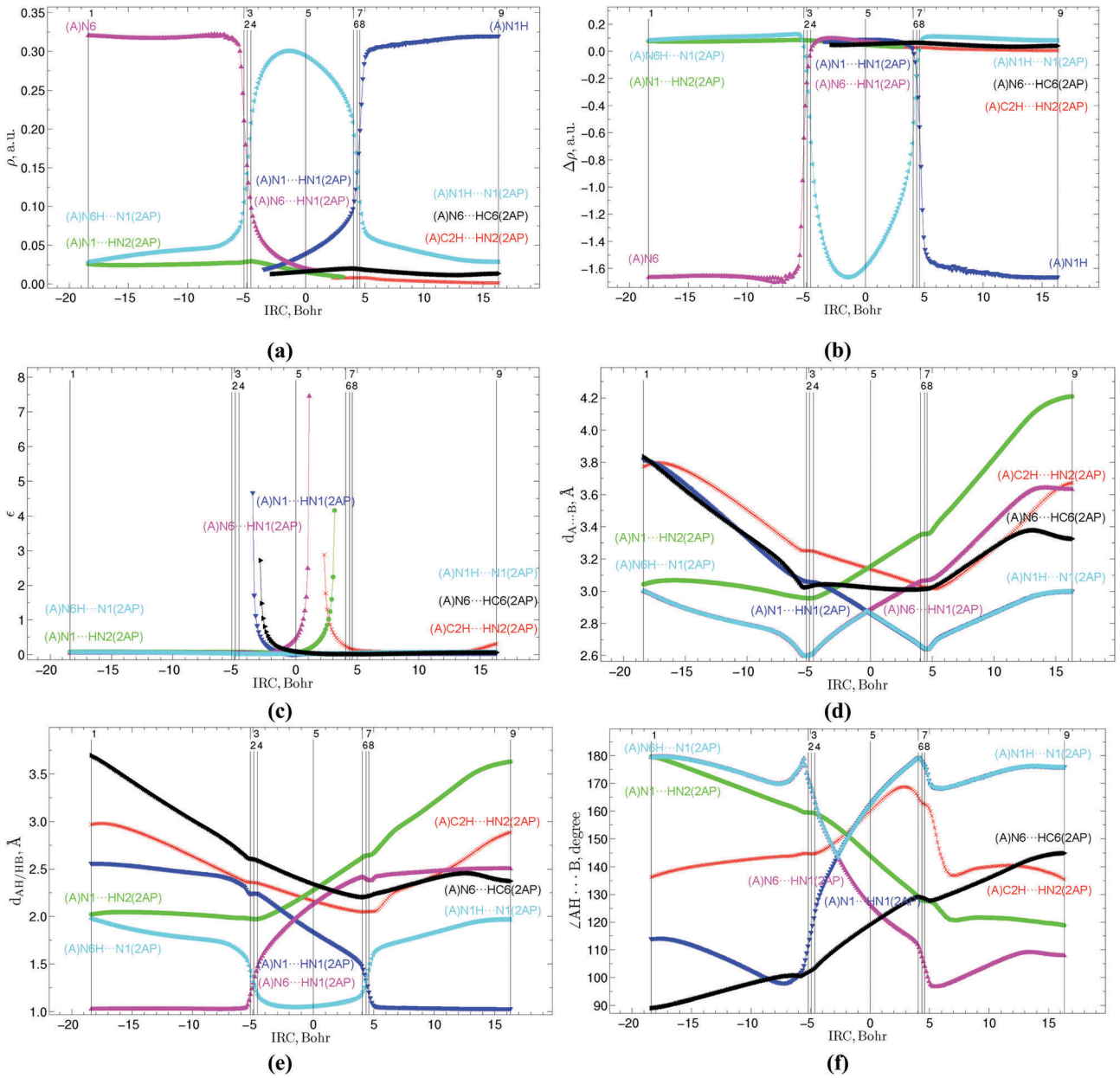

Fig. 7 Profiles of (a) electron density ρ; (b) Laplacian of the electron density $\Delta\rho$, (c) ellipticity ε at the (3,−1) BCPs, (d) distance $d_{A\cdots B}$ between the electronegative A and B atoms; (e) distance $d_{AH/HB}$ between the hydrogen and electronegative A or B atoms and (f) angle $\angle AH\cdots B$ of the AH···B H-bonds along the IRC of the A·2AP(w) ↔ A*·2AP(WC) w ↔ WC tautomerisation *via* the sequential PT obtained at the B3LYP/6-311++G(d,p) level of theory in the continuum with ε = 1.

are involved into the mutagenic G·2AP*(w) → G*·2AP(w) → G·2AP(WC) → G·2AP$_{syn}$[32,35] and A·2AP(w) → A*·2AP(WC) → A*·2AP$_{syn}$[33] tautomerically-conformational pathways originating from the induced transitions and transversions.

The profiles of the electronic energy E, the first derivative of the electronic energy with respect to the IRC, dE/dIRC, the dipole moment of the base pair μ, the NBO charges q_{NBO} of the hydrogen atoms involved in the tautomerisations, the distance $R(H_9–H_9)$ between the H_9 glycosidic hydrogens, the glycosidic angles α_1/α_2, the electron density ρ, the Laplacian of the electron density $\Delta\rho$ and the ellipticity ε at the (3,−1) BCPs of the intrapair covalent and hydrogen bonds, the distances $d_{A\cdots B}$, $d_{AH/HB}$, the angles $\angle AH\cdots B$ and the energy of the intermolecular H-bonds E_{HB} along the IRC were established.

This detailed analysis enabled us to follow all the changes in the physico-chemical characteristics, including energetic, structural, polar, charge, and electron-topological, along the IRC at each point of these reactions. Moreover, it was found that the G*·2AP(w) ↔ G·2AP(WC) and A·2AP(w) ↔ A*·2AP(WC) w ↔ WC tautomerisations proceed *via* the followed by the subsequent shifting of the G/A and 2AP bases relative to each other.

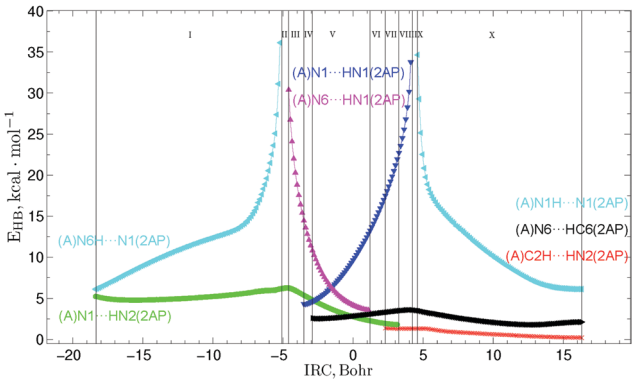

Fig. 8 Profiles of the energy of the intermolecular H-bonds E_{HB} estimated by the EML formula at the (3,−1) BCPs along the IRC of the A·2AP(w) ↔ A*·2AP(WC) w ↔ WC tautomerisation *via* the sequential PT obtained at the B3LYP/6-311++G(d,p) level of theory in the continuum with ε = 1 (see Table 5).

Nine key points along the IRC were established, three of them (1st, 5th and 9th) correspond to the stationary structures and the six others (2nd, 3rd, 4th, 6th, 7th and 8th) reflect the rearrangement of the intermolecular H-bonds, O6/N6H···N1, N2H···N1 (G*·2AP(w)/A·2AP(w)) → $C6^{+}H\cdots O6^{-}/N6^{-}$, $N1^{+}H\cdots O6^{-}/N6^{-}$, $N1^{+}H\cdots N1^{-}$, $N2^{+}H\cdots N1^{-}$, $N2^{+}H\cdots N2^{-}$ ($TS^{G^{-}\cdot 2AP^{+}}_{G^{*}\cdot 2AP(w)\leftrightarrow G\cdot 2AP(WC)}/TS^{A^{-}\cdot 2AP^{+}}_{A\cdot 2AP(w)\leftrightarrow A^{*}\cdot 2AP(WC)}$) → C6H···O6/N6, N1H···N1 and N2/C2H···N2/HN2 (G·2AP(WC)/A*·2AP(WC)), which are grouped into 10 patterns of interactions including AH···B H-bonds and loosened A–H–B covalent bridges.

Conflicts of interest

There are no conflicts to declare.

Acknowledgements

The authors gratefully appreciate technical support and computational facilities of joint computer cluster of SSI "Institute for Single Crystals" of the National Academy of Sciences of Ukraine (NASU) and Institute for Scintillation Materials of the NASU incorporated into the Ukrainian National Grid. This work was partially supported by the Grant of the NASU for young scientists for 2017 year, Grant of the President of Ukraine to support the research of young scientists [project number F70] from the State Fund for Fundamental Research of Ukraine of the Ministry of the Education and Science of Ukraine and by the Personal Scholarship of Verkhovna Rada (Parliament) of Ukraine for the talented young scientists in 2017 year given to DrSci Ol'ha O. Brovarets'. O. O. B. expresses sincere gratitude to organizing committee for financial support of the participation in the "EMBO/FEBS Lecture Course Spetsai Summer School 2017 for Proteins and Organized Complexity" (September 24–October 1, 2017, Spetses, Greece), to Lawyers Association "AVER Lex" (Kyiv, Ukraine) for the sponsorship of the presenting the plenary lecture as invited speaker at the "EMN Meeting on Computation and Theory" (November 6–10, 2017, Dubai, United Arab Emirates) and to Max Planck Institute of Plant Physiology (hosted by Dr. Yariv Brotman) for the invitation and financial support of the invited talk (November 29, 2017, Potsdam, Germany).

References

1 C. Janion, The efficiency and extent of mutagenic activity of some new mutagens of base-analogue type, *Mutat. Res.*, 1978, **56**, 225–234.
2 M. F. Goodman, S. Creighton, L. B. Bloom, J. Petruska and T. A. Kunkel, Biochemical basis of DNA replication fidelity, *Crit. Rev. Biochem. Mol. Biol.*, 1993, **28**, 83–126.
3 A. N. Nedderman, M. J. Stone, P. K. T. Lin, D. M. Brown and D. H. Williams, Base pairing of cytosine analogues with adenine and guanine in oligonucleotide duplexes: evidence for exchange between Watson–Crick and wobble base pairs using ^{1}H NMR spectroscopy, *J. Chem. Soc., Chem. Commun.*, 1991, 1357–1359.
4 A. N. Nedderman, M. J. Stone, D. H. Williams, P. K. Y. Lin and D. M. Brown, Molecular basis for methoxyamine-initiated mutagenesis: 1H nuclear magnetic resonance studies of oligonucleotide duplexes containing base-modified cytosine residues, *J. Mol. Biol.*, 1993, **230**, 1068–1076.
5 V. I. Danilov, T. van Mourik, N. Kurita, H. Wakabayashi, T. Tsukamoto and D. M. Hovorun, On the mechanism of the mutagenic action of 5-bromouracil: a DFT study of uracil and 5-bromouracil in a water cluster, *J. Phys. Chem. A*, 2009, **113**, 2233–2235.
6 C. S. Peng, B. I. Fedeles, V. Singh, D. Li, T. Amariuta, J. M. Essigmann and A. Tokmakoff, Two-dimensional IR spectroscopy of the anti-HIV agent KP1212 reveals protonated and neutral tautomers that influence pH-dependent mutagenicity, *Proc. Natl. Acad. Sci. U. S. A.*, 2015, **112**, 3229–3234.
7 Ch.W. Lawrence, Induced mutagenesis: molecular mechanisms and their implications for environmental protection, *Basic Life Sci.*, 1983, 433.
8 A. Hollaender, *Chemical mutagens: principles and methods for their detection, V.1*, Plenum Press, New York, 1971, p. 310.
9 M. J. Bessman, N. Muzyczka, M. F. Goodman and R. L. Schnaar, Studies on the biochemical basis of spontaneous mutation. II. The incorporation of a base and its analogue into DNA by wild-type, mutator and antimutator DNA polymerases, *J. Mol. Biol.*, 1974, **88**, 409–421.
10 R. Rein and R. Garduno, in *Energetics and mechanism of 2-aminopurine induced mutations chapter quantum science*, ed. J.-L. Calais, O. Goscinski, J. Linderberg and Y. Öhrn, Springer, 1976, pp. 549–560.
11 M. F. Goodman, R. Hopkins and W. C. Gore, 2-Aminopurine-induced mutagenesis in T4 bacteriophage: a model relating mutation frequency to 2-aminopurine incorporation in DNA, *Proc. Natl. Acad. Sci. U. S. A.*, 1977, **74**, 4806–4810.
12 A. Ronen, 2-Aminopurine, *Mutat. Res.*, 1979, **75**, 1–47.
13 S. M. Watanabe and M. F. Goodman, On the molecular basis of transition mutations: frequencies of forming 2-aminopurine·cytosine and adenine·cytosine base mispairs *in vitro*, *Proc. Natl. Acad. Sci. U. S. A.*, 1981, **78**, 2864–2868.

14 S. M. Watanabe and M. F. Goodman, Kinetic measurement of 2-aminopurine cytosine and 2-aminopurine thymine base pairs as a test of DNA polymerase fidelity mechanisms, *Proc. Natl. Acad. Sci. U. S. A.*, 1982, **79**, 6429–6433.

15 B. W. Glickman, 2-aminopurine mutagenesis in *Escherichia coli*, in *Genetic consequences of nucleotide pool imbalance. V.31 of the series Basic Life Sciences*, ed. F. J. de Serres, Springer, 1985, pp. 353–379.

16 L. C. Sowers, Y. Boulard and G. V. Fazakerley, Multiple structures for the 2-aminopurine-cytosine mispairs, *Biochemistry*, 2000, **39**, 7613–7620.

17 P. Pitsikas, J. M. Patapas and C. G. Cupples, Mechanism of 2-aminopurine-stimulated mutagenesis in *Escherichia coli*, *Mutat. Res.*, 2004, **550**, 25–32.

18 E. A. Alemán, C. de Silva, E. M. Patrick, K. Musier-Forsyth and D. Rueda, Single-molecule fluorescence using nucleotide analogs: a proof-of-principle, *J. Phys. Chem. Lett.*, 2014, **5**, 777–781.

19 A. Elvin, E. A. Alemán and D. Rueda, 2-Aminopurine single-molecule fluorescence, *Biophys. J.*, 2011, **100**(Suppl. 1), 474a.

20 C. Wan, T. Fiebig, O. Schiemann, J. K. Barton and A. H. Zewail, Femtosecond direct observation of charge transfer between bases in DNA, *Proc. Natl. Acad. Sci. U. S. A.*, 2000, **97**, 14052–14055.

21 E. L. Rachofsky, R. Osman and J. B. Ross, Probing structure and dynamics of DNA with 2-aminopurine: effects of local environment on fluorescence, *Biochemistry*, 2001, **40**, 946–949.

22 J. M. Jean and K. B. Hall, 2-Aminopurine fluorescence quenching and lifetimes: role of base stacking, *Proc. Natl. Acad. Sci. U. S. A.*, 2001, **98**, 37–41.

23 V. I. Danilov, Iu. A. Krugliak, V. A. Kuprievich and O. V. Shramko, O mekhanizme mutagennogo deistviia 2-aminopurina [According the mechanism of the mutagenic action of 2-aminopurine], *Biofizika*, 1967, **12**, 726–729.

24 A. Broo and A. Holmén, *Ab initio* MP2 and DFT calculations of geometry and solution tautomerism of purine and some purine derivatives, *Chem. Phys.*, 1996, **211**, 147–161.

25 E. C. Sherer and C. J. Cramer, Quantum chemical characterization of the cytosine: 2-aminopurine base pair, *J. Comput. Chem.*, 2001, **22**, 1167–1179.

26 R. Ramaekers, L. Adamowicz and G. Maes, Tautomery and H-bonding characteristics of 2-aminopurine: a combined experimental and theoretical study, *Eur. Phys. J. D*, 2002, **20**, 375–388.

27 O. O. Brovarets' and D. M. Hovorun, Molecular mechanisms of the mutagenic action of 2-aminopurine on DNA, *Ukr. Bioorg. Acta*, 2010, **9**, 11–17.

28 O. O. Brovarets' and D. M. Hovorun, IR vibrational spectra of H-bonded complexes of adenine, 2-aminopurine and 2-aminopurine^{+} with cytosine and thymine: quantum-chemical study, *Opt. Spectrosc.*, 2010, **111**, 750–757.

29 O. O. Brovarets', PhD thesis, *''Physico-chemical nature of the spontaneous and induced by the mutagens transitions and transversions''*, Taras Shevchenko National University of Kyiv, Kyiv, Ukraine, 2010.

30 O. O. Brovarets', DrSci thesis, *''Microstructural mechanisms of the origin of the spontaneous point mutations''*, Taras Shevchenko National University of Kyiv, Kyiv, Ukraine, 2015.

31 O. O. Brovarets', H. E. Pérez-Sánchez and D. M. Hovorun, Structural grounds for the 2-aminopurine mutagenicity: a novel insight into the old problem of the replication errors, *RSC Adv.*, 2016, **6**, 99546–99557.

32 O. O. Brovarets' and H. E. Pérez-Sánchez, Whether the amino-imino tautomerism of 2-aminopurine is involved into its mutagenicity? Results of a thorough QM investigation, *RSC Adv.*, 2016, **110**, 108255–108264.

33 O. O. Brovarets' and H. E. Pérez-Sánchez, Whether 2-aminopurine induces incorporation errors at the DNA replication? A quantum-mechanical answer on the actual biological issue, *J. Biomol. Struct. Dyn.*, 2017, **35**, 3398–3411.

34 O. O. Brovarets', I. S. Voiteshenko, H. E. Pérez-Sánchez and D. M. Hovorun, A QM/QTAIM detailed look at the Watson-Crick ↔ wobble tautomeric transformations of the 2-aminopurine·pyrimidine mispairs, *J. Biomol. Struct. Dyn.*, 2017, DOI: 10.1080/07391102.2017.1331864.

35 O. O. Brovarets', I. S. Voiteshenko, H. E. Pérez-Sánchez and D. M. Hovorun, A QM/QTAIM research under the magnifying glass of the DPT tautomerisation of the wobble mispairs involving 2-aminopurine, *New J. Chem.*, 2017, **41**, 7232–7243.

36 O. O. Brovarets' and D. M. Hovorun, New structural hypostases of the A·T and G·C Watson-Crick DNA base pairs caused by their mutagenic tautomerisation in a wobble manner: a QM/QTAIM prediction, *RSC Adv.*, 2015, **5**, 99594–99605.

37 O. O. Brovarets' and D. M. Hovorun, Tautomeric transition between wobble A·C DNA base mispair and Watson-Crick-like A·C* mismatch: microstructural mechanism and biological significance, *Phys. Chem. Chem. Phys.*, 2015, **17**, 15103–15110.

38 O. O. Brovarets' and D. M. Hovorun, By how many tautomerisation routes the Watson-Crick-like A·C* DNA base mispair is linked with the wobble mismatches? A QM/QTAIM vision from a biological point of view, *Struct. Chem.*, 2016, **27**, 119–131.

39 O. O. Brovarets' and D. M. Hovorun, How many tautomerisation pathways connect Watson-Crick-like G*·T DNA base mispair and wobble mismatches?, *J. Biomol. Struct. Dyn.*, 2015, **33**, 2297–2315.

40 O. H. O. Brovarets' and D. M. Hovorun, Wobble ↔ Watson-Crick tautomeric transitions in the homo-purine DNA mismatches: a key to the intimate mechanisms of the spontaneous transversions, *J. Biomol. Struct. Dyn.*, 2015, **33**, 2710–2715.

41 O. O. Brovarets' and D. M. Hovorun, Novel physico-chemical mechanism of the mutagenic tautomerisation of the Watson–Crick-like A·G and C·T DNA base mispairs: a quantum-chemical picture, *RSC Adv.*, 2015, **5**, 66318–66333.

42 O. O. Brovarets' and D. M. Hovorun, A novel conception for spontaneous transversions caused by homo-pyrimidine DNA mismatches: a QM/QTAIM highlight, *Phys. Chem. Chem. Phys.*, 2015, **17**, 21381–21388.

43 J. D. Watson and F. H. C. Crick, The structure of DNA, *Cold Spring Harbor Symp. Quant. Biol.*, 1953, **18**, 123–131.

44 M. M. Huang, N. Arnheim and M. F. Goodman, Extension of base mispairs by Taq DNA polymerase: implications for single nucleotide discrimination in PCR, *Nucleic Acids Res.*, 1992, **20**, 4567–4573.

45 M. Lynch, Rate, molecular spectrum, and consequences of human mutation, *Proc. Natl. Acad. Sci. U. S. A.*, 2010, **107**, 961–968.

46 H. Lee, E. Popodi, H. Tang and P. L. Foster, Extension of base mispairs by Taq DNA polymerase: implications for single nucleotide discrimination in PCR, *Nucleic Acids Res.*, 2012, **20**, 4567–4573.

47 I. J. Kimsey, K. Petzold, B. Sathyamoorthy, Z. W. Stein and H. M. Al-Hashimi, Visualizing transient Watson-Crick-like mispairs in DNA and RNA duplexes, *Nature*, 2015, **519**, 315–320.

48 E. S. Szymanski, I. J. Kimsey and H. M. Al-Hashimi, Direct NMR evidence that transient tautomeric and anionic states in dG·dT form Watson–Crick-like base pairs, *J. Am. Chem. Soc.*, 2017, **139**, 4326–4329.

49 O. O. Brovarets' and D. M. Hovorun, Quantum-chemical investigation of tautomerization ways of Watson-Crick DNA base pair guanine-cytosine, *Ukr. Biochem. J.*, 2010, **82**, 55–60.

50 O. O. Brovarets' and D. M. Hovorun, Quantum-chemical investigation of the elementary molecular mechanisms of pyrimidine·purine transversions, *Ukr. Biochem. J.*, 2010, **82**, 57–67.

51 O. O. Brovarets, R. O. Zhurakivsky and D. M. Hovorun, Is there adequate ionization mechanism of the spontaneous transitions? Quantum-chemical investigation, *Biopolym. Cell*, 2010, **26**, 398–405.

52 O. O. Brovarets' and D. M. Hovorun, Intramolecular tautomerization and the conformational variability of some classical mutagens – cytosine derivatives: Quantum chemical study, *Biopolym. Cell*, 2011, **27**, 221–230.

53 O. O. Brovarets' and D. M. Hovorun, Does the G·G*$_{syn}$ DNA mismatch containing canonical and rare tautomers of the guanine tautomerise through the DPT? A QM/QTAIM microstructural study, *Mol. Phys.*, 2014, **112**, 3033–3046.

54 Ya.R Mishchuk, A. L. Potyagaylo and D. M. Hovorun, Structure and dynamics of 6-azacytidine by MNDO/H quantum-chemical method, *J. Mol. Struct.*, 2000, **552**, 283–289.

55 I. V. Kondratyuk, S. P. Samijlenko, I. M. Kolomiets' and D. M. Hovorun, Prototropic molecular-zwitterionic tautomerism of xanthine and hypoxanthine, *J. Mol. Struct.*, 2000, **523**, 109–118.

56 S. P. Samijlenko, O. M. Krechkivska, D. A. Kosach and D. M. Hovorun, Transitions to high tautomeric states can be induced in adenine by interactions with carboxylate and sodium ions: DFT calculation data, *J. Mol. Struct.*, 2004, **708**, 97–104.

57 M. O. Platonov, S. P. Samijlenko, O. O. Sudakov, I. V. Kondratyuk and D. M. Hovorun, To what extent can methyl derivatives be regarded as stabilized tautomers of xanthine?, *Spectrochim. Acta, Part A*, 2005, **62**, 112–114.

58 M. J. Frisch, G. W. Trucks, H. B. Schlegel, G. E. Scuseria, M. A. Robb, J. R. Cheeseman and J. A. Pople, *GAUSSIAN 09 (Revision B.01)*, Gaussian Inc., Wallingford CT, 2010.

59 M. A. Palafox, Molecular structure differences between the antiviral nucleoside analogue 5-iodo-2′-deoxyuridine and the natural nucleoside 2′-deoxythymidine using MP2 and DFT methods: conformational analysis, crystal simulations, DNA pairs and possible behavior, *J. Biomol. Struct. Dyn.*, 2014, **32**, 831–851.

60 A. A. El-Sayed, A. Tamara Molina, M. C. Alvarez-Ros and M. Alcolea Palafox, Conformational analysis of the anti-HIV Nikavir prodrug: comparisons with AZT and thymidine, and establishment of structure-activity relationships/tendencies in other 6′-derivatives, *J. Biomol. Struct. Dyn.*, 2015, **33**, 723–748.

61 M. Cossi, N. Rega, G. Scalmani and V. Barone, Energies, structures, and electronic properties of molecules in solution with the C-PCM solvation model, *J. Comput. Chem.*, 2003, **24**, 669–681.

62 V. Barone and M. Cossi, Quantum calculation of molecular energies and energy gradients in solution by a conductor solvent model, *J. Phys. Chem. A*, 1998, **102**, 1995–2001.

63 E. L. Mertz and L. I. Krishtalik, Low dielectric response in enzyme active site, *Proc. Natl. Acad. Sci. U. S. A.*, 2000, **97**, 2081–2086.

64 J. Petrushka, L. C. Sowers and M. Goodman, Comparison of nucleotide interactions in water, proteins, and vacuum: Model for DNA polymerase fidelity, *Proc. Natl. Acad. Sci. U. S. A.*, 1986, **83**, 1559–1562.

65 H. P. Hratchian and H. B. Schlegel, Finding minima, transition states, and following reaction pathways on ab initio potential energy surfaces, in *Theory and applications of computational chemistry: The first 40 years*, ed. Dykstra C. E., Frenking G., Kim K. S. and Scuseria G., Amsterdam, Elsevier, 2005, pp. 195–249.

66 O. O. Brovarets' and D. M. Hovorun, Can tautomerisation of the A·T Watson–Crick base pair *via* double proton transfer provoke point mutations during DNA replication? A comprehensive QM and QTAIM analysis, *J. Biomol. Struct. Dyn.*, 2014, **32**, 127–154.

67 O. O. Brovarets' and D. M. Hovorun, Why the tautomerization of the G·C Watson–Crick base pair *via* the DPT does not cause point mutations during DNA replication? QM and QTAIM comprehensive analysis, *J. Biomol. Struct. Dyn.*, 2014, **32**, 1474–1499.

68 O. O. Brovarets', R. O. Zhurakivsky and D. M. Hovorun, DPT tautomerisation of the wobble guanine·thymine DNA base mispair is not mutagenic: QM and QTAIM arguments, *J. Biomol. Struct. Dyn.*, 2015, **33**, 674–689.

69 O. O. Brovarets' and D. M. Hovorun, The physicochemical essence of the purine·pyrimidine transition mismatches with Watson-Crick geometry in DNA: A·C* versa A*·C. A QM and QTAIM atomistic understanding, *J. Biomol. Struct. Dyn.*, 2015, **33**, 28–55.

70 O. O. Brovarets' and D. M. Hovorun, The nature of the transition mismatches with Watson-Crick architecture: the

G*·T or G·T* DNA base mispair or both? A QM/QTAIM perspective for the biological problem, *J. Biomol. Struct. Dyn.*, 2015, **33**, 925–945.

71 *NBO, 3.1*, ed. Glendening E. D., Reed A. E., Carpenter J. E. and Weinhold F., Theoretical Chemistry Institute, University of Wisconsin, Madison, WI, 1994.

72 R. F. W. Bader, *Atoms in molecules: a quantum theory*, Oxford University Press, Oxford, 1990.

73 T. A. Keith, AIMAll (Version 10.07.01), 2010, Retrieved from aim.tkgristmill.com.

74 C. F. Matta and J. Hernández-Trujillo, Bonding in polycyclic aromatic hydrocarbons in terms of the electron density and of electron delocalization, *J. Phys. Chem. A*, 2005, **109**, 10798.

75 E. Espinosa, E. Molins and C. Lecomte, Hydrogen bond strengths revealed by topological analyses of experimentally observed electron densities, *Chem. Phys. Lett.*, 1998, **285**, 170–173.

76 I. Mata, I. Alkorta, E. Espinosa and E. Molins, Relationships between interaction energy, intermolecular distance and electron density properties in hydrogen bonded complexes under external electric fields, *Chem. Phys. Lett.*, 2011, **507**, 185–189.

77 W. Saenger, *Principles of nucleic acid structure*, Springer, New York, 1984.

78 J. C. Hargis, E. Vöhringer-Martinez, H. L. Woodcock, A. Toro-Labbé and H. F. Schaefer, 3rd, Characterizing the mechanism of the double proton transfer in the formamide dimer, *J. Phys. Chem. A*, 2011, **115**, 2650–2657.

79 F. Duarte, E. Vöhringer-Martinez and A. Toro-Labbé, Insights on the mechanism of proton transfer reactions in amino acids, *Phys. Chem. Chem. Phys.*, 2011, **13**, 7773–7782.

80 D. Guzmán-Angel, R. Inostroza-Rivera, S. Gutiérrez-Oliva, B. Herrera and A. Toro-Labbé, Role of water in intramolecular proton transfer reactions of formamide and thioformamide, *Theor. Chem. Acc.*, 2016, **135**, 37.

81 O. O. Brovarets' and D. M. Hovorun, DPT tautomerization of the long A·A* Watson-Crick base pair formed by the amino and imino tautomers of adenine: combined QM and QTAIM investigation, *J. Mol. Model.*, 2013, **19**, 4223–4237.

82 O. O. Brovarets', R. O. Zhurakivsky and D. M. Hovorun, Structural, energetic and tautomeric properties of the T·T*/T*·T DNA mismatch involving mutagenic tautomer of thymine: a QM and QTAIM insight, *Chem. Phys. Lett.*, 2014, **592**, 247–255.

83 O. O. Brovarets' and D. M. Hovorun, How does the long G·G* Watson-Crick DNA base mispair comprising keto and enol tautomers of the guanine tautomerise? The results of a QM/QTAIM investigation, *Phys. Chem. Chem. Phys.*, 2014, **16**, 15886–15899.

84 O. O. Brovarets', R. O. Zhurakivsky and D. M. Hovorun, Is the DPT tautomerisation of the long A·G Watson-Crick DNA base mispair a source of the adenine and guanine mutagenic tautomers? A QM and QTAIM response to the biologically important question, *J. Comput. Chem.*, 2014, **35**, 451–466.

85 O. O. Brovarets' and D. M. Hovorun, DPT tautomerisation of the G·A_{syn} and A*·G^*_{syn} DNA mismatches: a QM/QTAIM combined atomistic investigation, *Phys. Chem. Chem. Phys.*, 2014, **16**, 9074–9085.

86 T. Y. Nikolaienko, L. A. Bulavin and D. M. Hovorun, How flexible are DNA constituents? The quantum-mechanical study, *J. Biomol. Struct. Dyn.*, 2011, **29**, 563–575.

87 D. M. Hovorun, L. Gorb and J. Leszczynski, From the nonplanarity of the amino group to the structural nonrigidity of the molecule: a post-Hartree-Fock *ab initio* study of 2-aminoimidazole, *Int. J. Quantum Chem.*, 1999, **75**, 245–253.

88 D. N. Govorun, V. D. Danchuk, Ya.R. Mishchuk, I. V. Kondratyuk, N. F. Radomsky and N. V. Zheltovsky, AM1 calculation of the nucleic acid bases structure and vibrational spectra, *J. Mol. Struct.*, 1992, **267**, 99–103.

